

Supplement of Atmos. Meas. Tech., 12, 3825–3839, 2019
<https://doi.org/10.5194/amt-12-3825-2019-supplement>
© Author(s) 2019. This work is distributed under
the Creative Commons Attribution 4.0 License.



Supplement of

Method to retrieve cloud condensation nuclei number concentrations using lidar measurements

Wangshu Tan et al.

Correspondence to: Chengcai Li (ccli@pku.edu.cn)

The copyright of individual parts of the supplement might differ from the CC BY 4.0 License.

S1 Site information

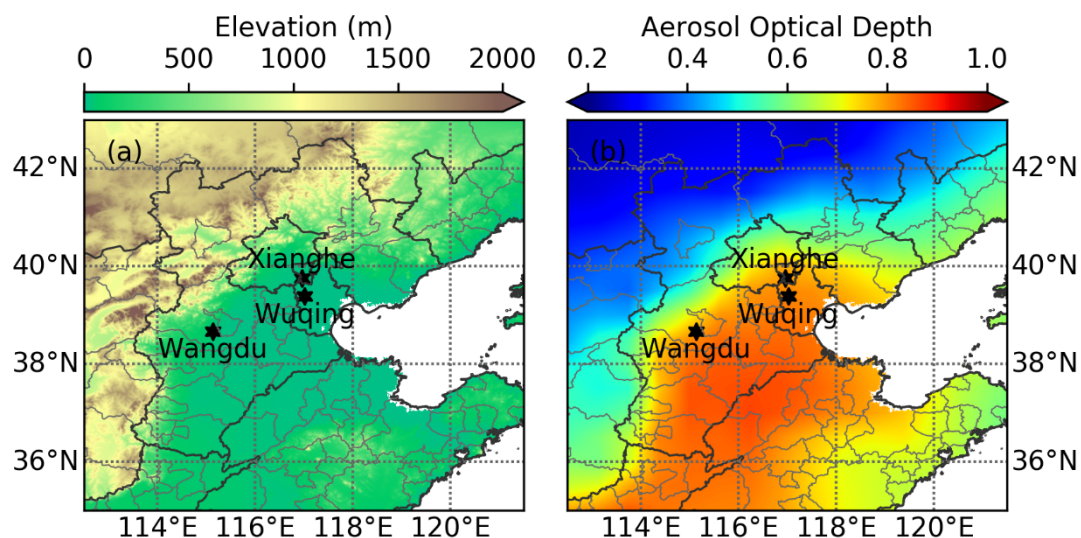


Figure S1. Site locations of Wuqing (39°23'N, 117°01'E, 7.4 m a.s.l), Xianghe (39°45'N, 116°58'E, 36 m a.s.l), and Wangdu (38°40'N, 115°08'E, 51 m a.s.l). Filled colors represents (a) elevation and (b) averaged aerosol optical depth (AOD). The AOD data is from reanalysis datasets of the Modern-Era Retrospective Analysis for Research and Applications, Version 2 (MERRA-2, Global Modeling and Assimilation Office (GMAO) (2015), MERRA-2 instM_2d_gas_Nx: 2d,Monthly mean,Instantaneous,Single-Level,Assimilation,Aerosol Optical Depth Analysis V5.12.4, Greenbelt, MD, USA, Goddard Earth Sciences Data and Information Services Center (GES DISC), Accessed: [11 September 2018], 10.5067/XOGNBQEPLUC5). The averaged AOD is calculated from monthly mean values of all months during the five field campaigns shown in Table 1.

S2 Time series of the normalized particle number size distribution (PNSD)

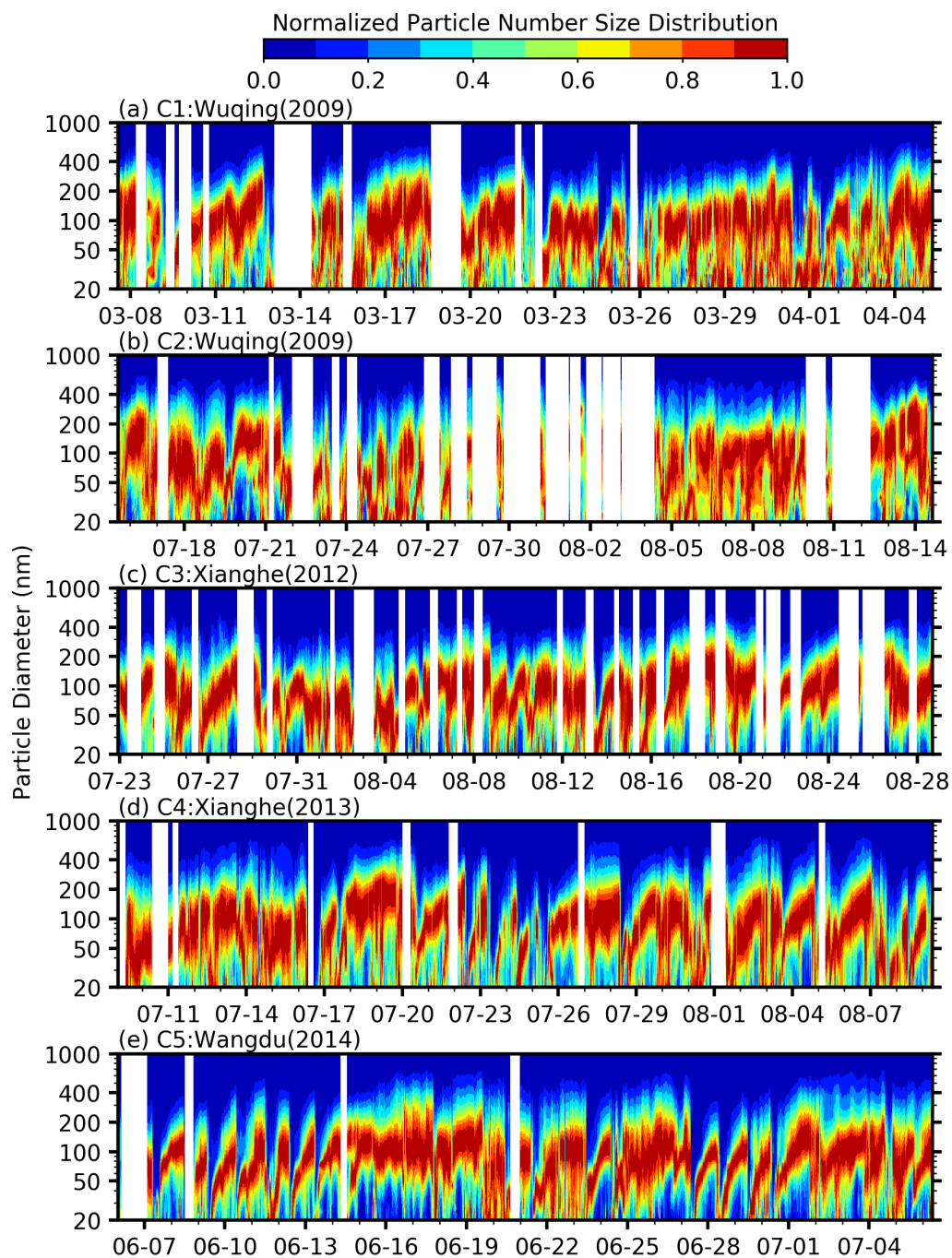


Figure S2. Time series of the normalized particle number size distribution from the five field campaigns. (a)-(e) represents campaign C1-C5, respectively.

S3 Theoretical simulations of CCN, lidar backscatter, and extinction

S3.1 Aerosol model assumptions

We assume the aerosol particles act as follows:

- (1) Aerosol particles are spherical, which means the simulation results are not appropriate for mineral dust.
- 5 (2) Particles are partially externally mixed and partially core-shell mixed. Only two kinds of aerosols are contained: pure black carbon (BC) and BC coated by non-light-absorbing components. Note that if $r_{\text{ext}} = 1$, there exists pure BC and pure non-light-absorbing particles. r_{ext} is defined with Eq. (2) in the paper.
- (3) The shape of BC mass size distribution (BCMSD) remains unchanged and the amount is related to the total BC mass concentration (m_{BC}). The fixed distribution comes from the average BCMSD obtained from Berner impactor measurements
- 10 (Ma et al., 2012) and is shown in Fig. S3.

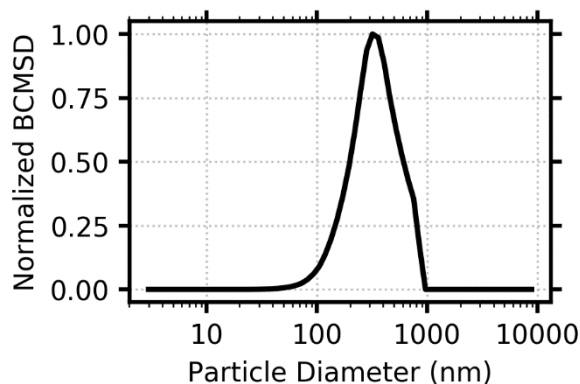


Figure S3. Normalized size distribution of black carbon (BC) mass/volume concentration. The distribution is the average black carbon mass concentration obtained from Berner impactor measurements (Ma et al., 2012) and is normalized by the maximum value of the distribution.

15

- (4) r_{ext} is uniform among different particle sizes. Accordingly, number concentrations of externally mixed BC (N_{ext}) can easily be calculated from BCMSD and r_{ext} :

$$N_{\text{ext}}(D) = \frac{r_{\text{ext}} \cdot m_{\text{BC}}(D)}{\frac{\pi}{6} D^3 \cdot \rho_{\text{BC}}}, \quad (\text{S1})$$

where D is diameter of the particle, ρ_{BC} is the density of BC. In this study, ρ_{BC} is assumed to be 1.5 g/cm^3 , which is also the

20 density when retrieving r_{ext} .

- (5) For each particle size, the diameters of BC cores (D_{core}) are the same and can be derived using the following equation:

$$D_{\text{core}}(D) = \sqrt[3]{\frac{6(1-r_{\text{ext}}) \cdot m_{\text{BC}}(D)}{\pi \rho_{\text{BC}} \cdot [N(D) - N_{\text{ext}}(D)]}}, \quad (\text{S2})$$

where $N(D)$ represents particle number size distribution (PNSD).

(6) The size-resolved κ distributions represent the bulk hygroscopicity of core-shell mixed particles, and externally mixed BC particles do not take up water.

All these assumptions above are strong and, to some extent, inconsistent with the reality, but are certified to be reasonable for calculating aerosol optical properties. Plenty of works on aerosol optical closure studies (Ma et al., 2011; Ma et al., 2012) and aerosol optical simulations (Kuang et al., 2017; Kuang et al., 2018; Zhao et al., 2018) have been carried out with these aerosol model assumptions. In particular, Zhao et al. (2017) use the aerosol model to simulate lidar backscatter and extinction under different relative humidity (RH) conditions.

S3.2 Calculations of CCN number concentrations using κ -Köhler theory

According to κ -Köhler theory, CCN number concentrations at a specific supersaturation level can be calculated by PNSD and size-resolved κ distribution. Based on Eq. (3), the critical supersaturation ratio required to activate a particle is decided by corresponding κ and D_{dry} . In other word, we can get a critical activation dry diameter D_c with a given supersaturation ratio and size-resolved κ distribution. Then CCN number concentration $N_{\text{CCN}}(SS)$ thereby can be calculated with Eq. (S3):

$$N_{\text{CCN}}(SS) = \int_{D_c(SS)}^{D_{\text{max}}} [N(D) - N_{\text{ext}}(D)] dD, \quad (\text{S3})$$

where D_{max} correspond to the upper bounds of the measured PNSD. Note that we regard externally mixed pure BC as non-hygroscopic particles, so r_{ext} and m_{BC} should also be involved to calculate N_{ext} , which needs to be subtracted. Otherwise, N_{CCN} will be overestimated.

S3.3 Calculations of particle backscatter and extinction coefficients at different RH using κ -Köhler theory and Mie theory

We use a modified BHMIE Fortran code and a modified BHCOAT Fortran code to calculate optical properties of homogeneous spherical particles and coated spherical particles, respectively. For a homogeneous spherical particle (i.e. externally mixed BC in this study), BHMIE can calculate particle scattering and extinction efficiency (Q_{sca} and Q_{ext}) and scattering phase function with given light wavelength, particle diameter, and complex refractive index. For a coated spherical particle (i.e. core-shell mixed particle), diameters and complex refractive indices of both core and shell are needed in BHCOAT. The particle backscatter and extinction coefficients we need are derived from Q_{sca} , Q_{ext} , and scattering phase function at 180° $P(\pi)$:

$$\alpha = \sum_i \left[\int_{D_{\text{min}}}^{D_{\text{max}}} \frac{1}{4} D^2 Q_{\text{ext}}(D, i) N(D, i) dD \right], \quad (\text{S4})$$

$$\beta = \sum_i \left[\int_{D_{\text{min}}}^{D_{\text{max}}} \frac{1}{16} D^2 Q_{\text{sca}}(D, i) P(\pi, D, i) N(D, i) dD \right], \quad (\text{S5})$$

where D_{min} and D_{max} correspond respectively to the lower and upper bounds of the measured PNSD, and the index i indicates the mixing state of particles, i.e. external or core-shell in this paper. Polarization of lidar emitted laser is neglected.

Complex refractive indices are essential for Mie scattering calculation. Aerosol complex refractive indices are related to chemical components, morphology, and wavelengths of light (Cotterell et al., 2017). Both real part and imaginary part of refractive indices vary a lot in real ambient environment (Shettle and Fenn, 1979). Wavelength dependency of refractive indices

at wavelengths of 355 nm, 532 nm, and 1064 nm are not significant except for brown carbon (Shettle and Fenn, 1979; Bond et al., 2013). Neglecting the effect of brown carbon in this study, we simply assume that complex refractive indices of corresponding components do not change with wavelengths. The refractive indices of BC and non-light-absorbing component (shell) are set to be $1.8+0.54i$ (Ma et al., 2012) and $1.53+10^{-7}i$ (Wex et al., 2002), respectively.

- 5 Concerning aerosol hygroscopicity for core-shell mixed particles, diameters of BC cores D_{core} remain unchanged, and particle diameters D at different RH can be calculated with Eq. (3). The refractive index of the swelling shell (\tilde{m}_{shell}) is calculated following the volume mixing law (Hanel, 1968):

$$\tilde{m}_{\text{shell}} = f_{\text{solute}} \cdot \tilde{m}_{\text{solute}} + (1 - f_{\text{solute}}) \cdot \tilde{m}_{\text{water}}, \quad (\text{S6})$$

- where $\tilde{m}_{\text{solute}}$ is the refractive index of solute (i.e. $1.53+10^{-7}i$ in this study), \tilde{m}_{water} is the refractive index of pure water ($1.33+10^{-7}i$), and f_{solute} is the solute volume fraction of the in solution (shell), which is determined by Eq. (S7):

$$f_{\text{solute}} = \frac{D_{\text{dry}}^3 - D_{\text{core}}^3}{D^3 - D_{\text{core}}^3}. \quad (\text{S7})$$

S4 Performance of fitting humidogram functions with parameterization equations

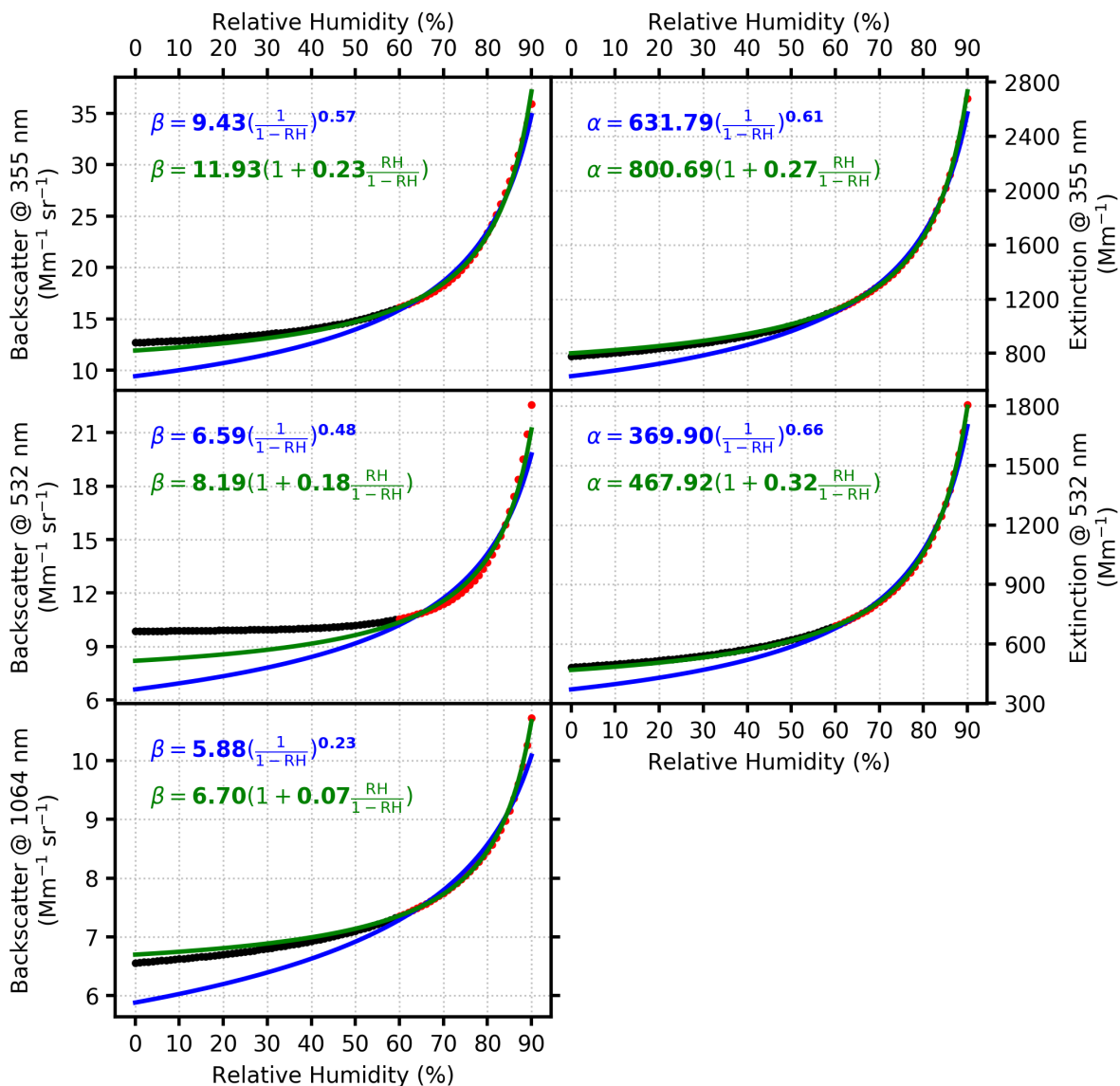


Figure S4. Example of humidogram fitting using different functions. The example is calculated with one set of PNSD, BC, r_{ext} , and size-resolved κ distribution. The dots represent Mie model simulations, and the dots in red (within RH range of 60-90%) are used to fit parameterization lines. The blue line is the result of γ -equation, and the green line represents the result of κ -equation.

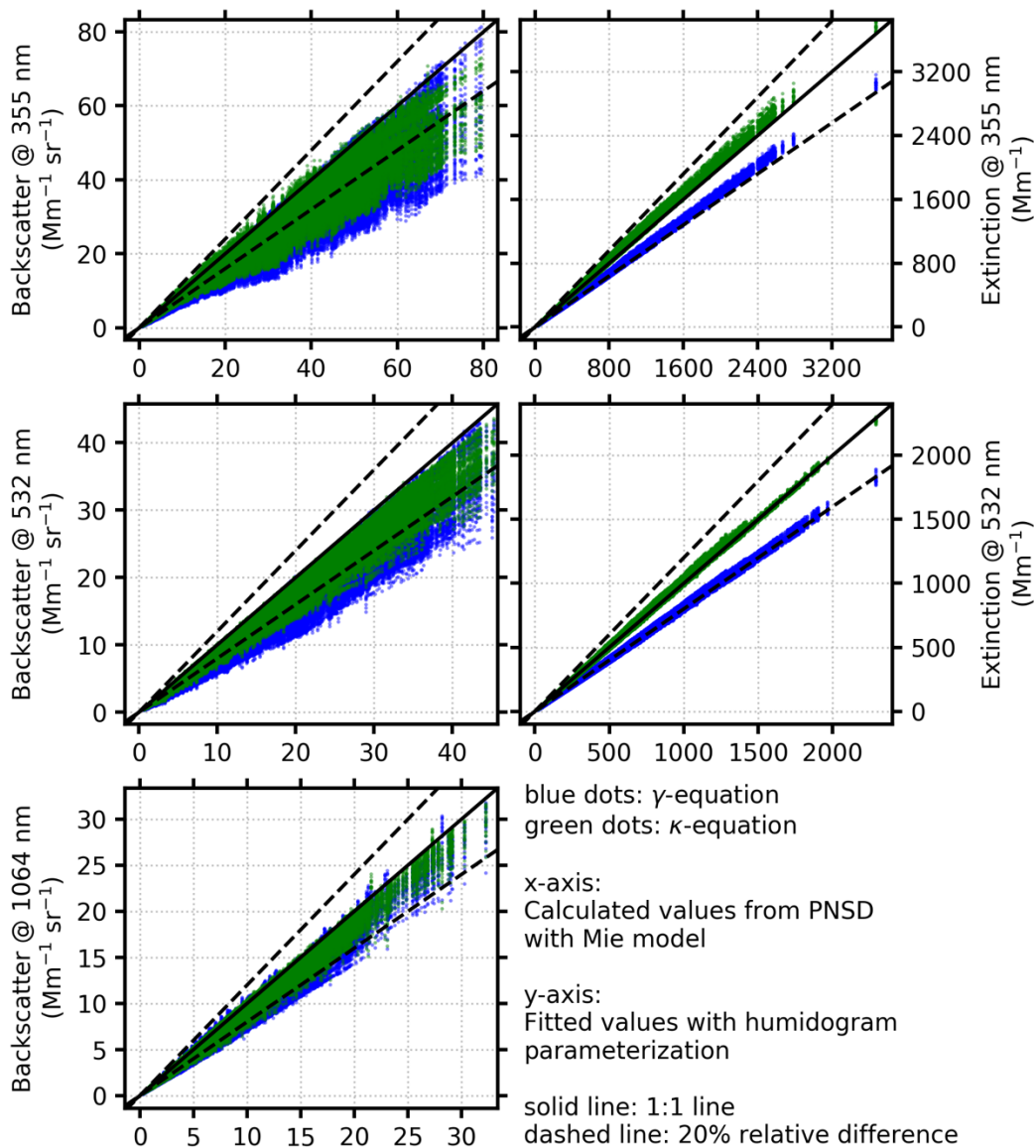


Figure S5. Comparison between Mie model calculated dry particle backscatter or extinction and those fitted from humidograms.

S5 Relationship between the nine input parameters in Table 4

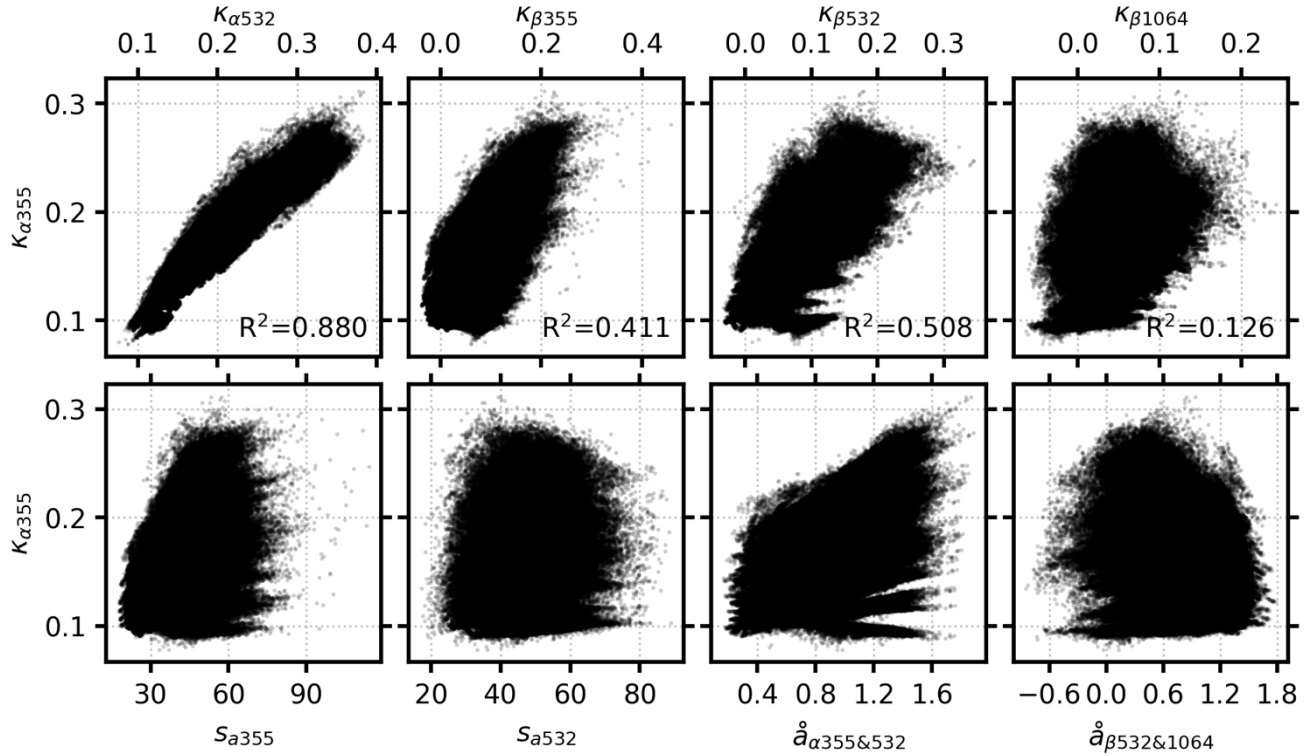


Figure S6. Relationship between $\kappa_{\alpha355}$ and other 8 parameters.

5 Table S1. Determine coefficients (R2) between the 9 input parameters in Table 4.

R^2	$\kappa_{\alpha355}$	$\kappa_{\alpha532}$	$\kappa_{\beta355}$	$\kappa_{\beta532}$	$\kappa_{\beta1064}$	S_{a355}	S_{a532}	$\dot{a}_{\alpha355\&532}$
$\kappa_{\alpha355}$	–	–	–	–	–	–	–	–
$\kappa_{\alpha532}$	0.880	–	–	–	–	–	–	–
$\kappa_{\beta355}$	0.411	0.321	–	–	–	–	–	–
$\kappa_{\beta532}$	0.508	0.644	0.450	–	–	–	–	–
$\kappa_{\beta1064}$	0.126	0.222	0.016	0.056	–	–	–	–
S_{a355}	0.085	0.073	0.680	0.292	0.019	–	–	–
S_{a532}	0.026	0.070	0.117	0.423	0.070	0.360	–	–
$\dot{a}_{\alpha355\&532}$	0.149	0.135	0.505	0.267	0.027	0.627	0.089	–
$\dot{a}_{\beta532\&1064}$	0.062	0.023	0.550	0.169	0.464	0.409	0.023	0.317

S6 Determine the tuning parameters for Random Forest model

In this study, we use the Python module *RandomForestRegressor* from the Python Scikit-Learn library (<http://scikit-learn.org/stable/modules/generated/sklearn.ensemble.RandomForestRegressor.html>, last access: 18 December 2018) as the Random Forest (RF) model tool. The tuning parameters of the model are listed in Table S2. More detailed meanings about the setting values please refer to the user guide provided by the website.

The most import tuning parameter in the model is the number of trees in the forest ($n_estimators$). The influence of $n_estimators$ on the accuracy of retrieved CCN number concentrations is tested. Here we use the same test method as introduced in Section 4.2 in the paper. The determination coefficients (R^2) and the mean absolute relative error (MARE) between theoretical calculated and retrieved CCN number concentrations with different $n_estimators$ are shown in Fig. S7.

10 The accuracy of the predictions increases as $n_estimators$ grows bigger and are insensitive when $n_estimators$ is bigger than 60. Considering computational and time cost, we finally set $n_estimators$ to 100.

Table S2. Tuning parameters and their setting values of the Python module *RandomForestRegressor*.

Parameter	Description	Values
$n_estimators$	The number of trees in the forest	100
$criterion$	The function to measure the quality of a split	“mse”
$max_features$	The number of features to consider when looking for the best split	“auto”
max_depth	The maximum depth of the tree	None
$min_samples_split$	The minimum number of samples required to split an internal node	2
$min_samples_leaf$	The minimum number of samples required to be at a leaf node	1
$min_weight_fraction_leaf$	The minimum weighted fraction of the sum total of weights (of all the input samples) required to be at a leaf node	0
max_leaf_nodes	Grow trees with max_leaf_nodes in best-first fashion	None
$min_impurity_decrease$	A node will be split if this split induces a decrease of the impurity greater than or equal to this value	0

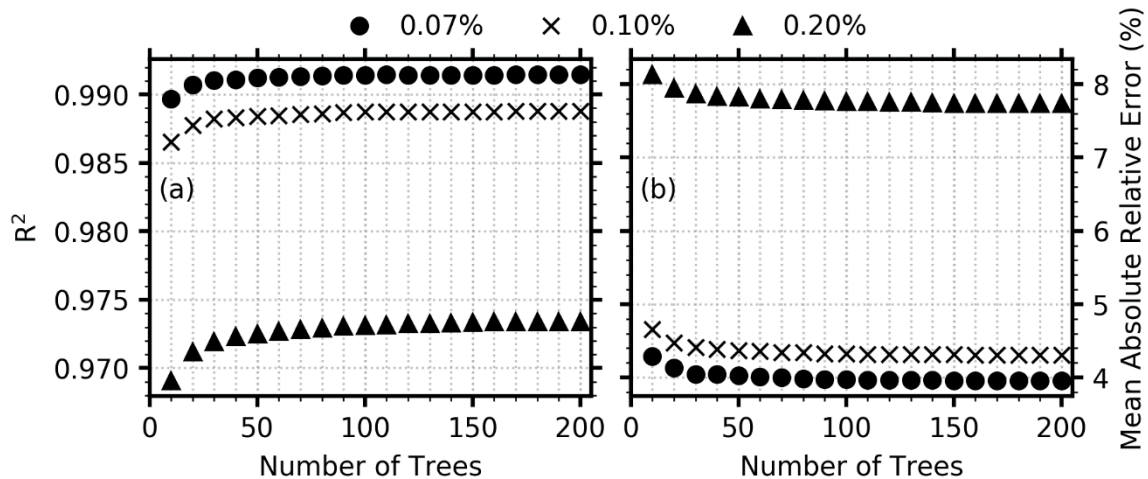


Figure S7. Influence of the number of trees in RF model on retrieving CCN number concentrations. Dependencies of tree numbers on (a) R^2 and (b) MARE between theoretical calculated CCN number concentrations and retrieved CCN number concentrations under different supersaturations.

S7 Retrieving CCN number concentrations at high supersaturations

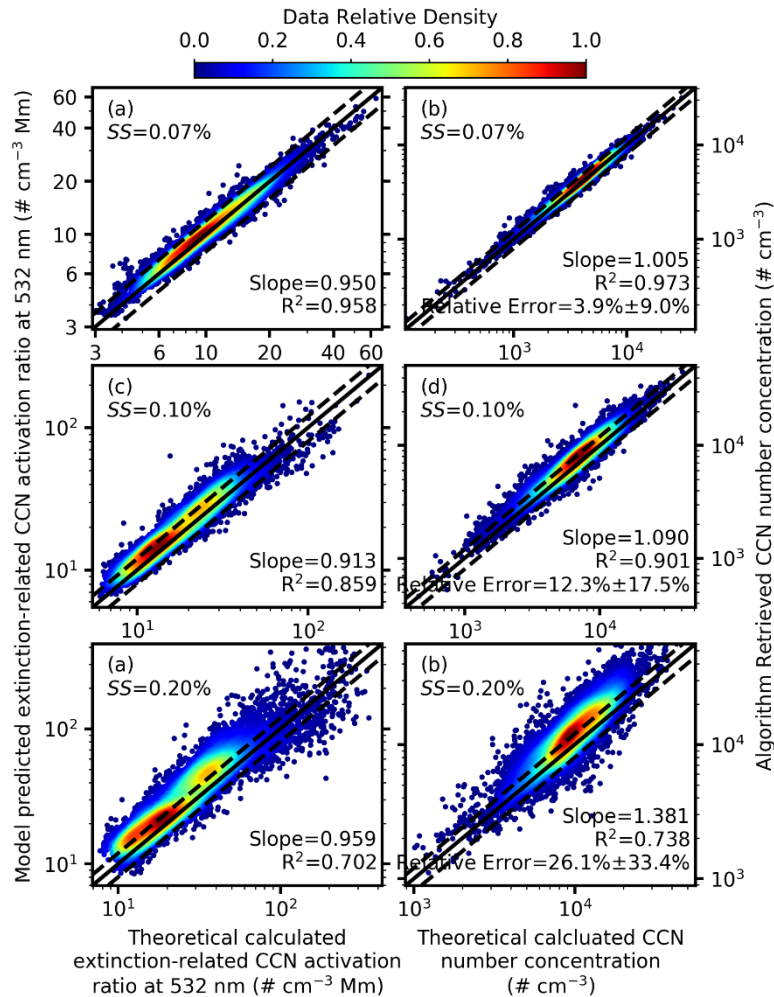


Figure S8. Comparison of the theoretical calculated extinction-related CCN activation ratio at 532 nm and the model predicted extinction-related CCN activation ratios at 532 nm at supersaturations of **(a)** 0.20%, **(c)** 0.40%, and **(e)** 0.80%, and of the theoretical calculated CCN number concentrations and the retrieved CCN number concentrations at supersaturations of **(b)** 0.20%, **(d)** 0.40%, and **(f)** 0.80%. A total of 80575 pairs of data calculated from campaign C5 are used. The solid line is 1:1 line, and the dashed lines are 20% relative difference lines. Colors represent the relative density of the data points normalized by the maximum data density of each panel. The relative error showed in the figure is mean value \pm one standard deviation.

S8 Retrieving CCN number concentrations without hygroscopicity information

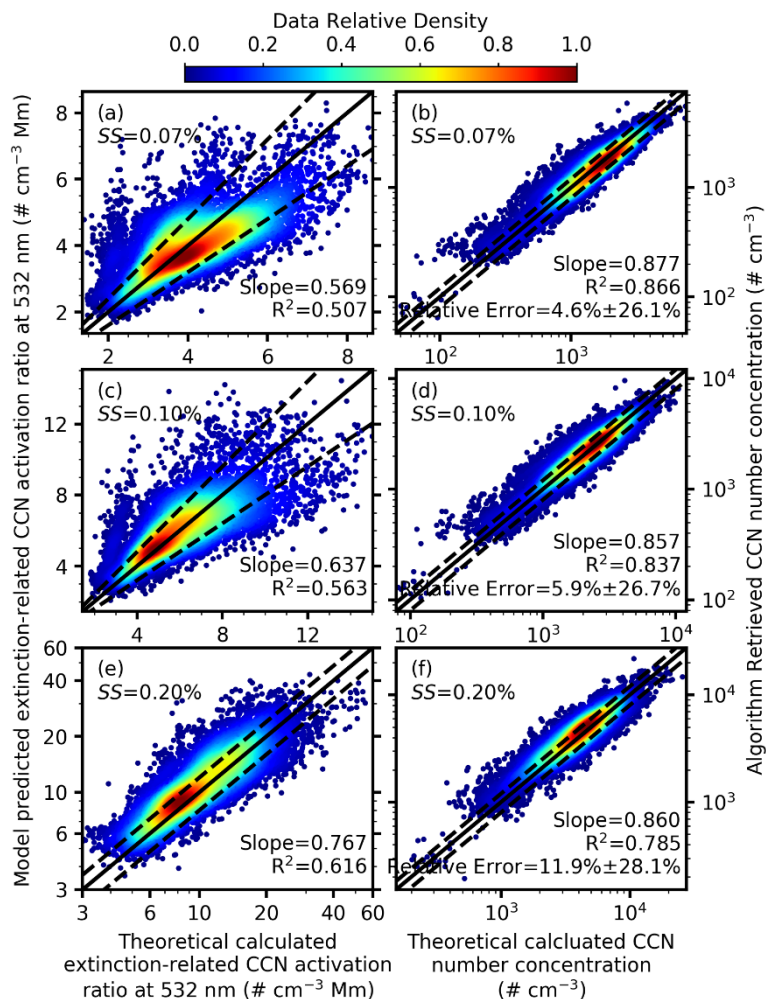


Figure S9. Comparison of the theoretical calculated extinction-related CCN activation ratio at 532 nm and the model predicted extinction-related CCN activation ratios at 532 nm at supersaturations of **(a)** 0.07%, **(c)** 0.10%, and **(e)** 0.20%, and of the theoretical calculated CCN number concentrations and the retrieved CCN number concentrations at supersaturations of **(b)** 0.07%, **(d)** 0.10%, and **(f)** 0.20%. A total of 80575 pairs of data calculated from campaign C5 are used. The solid line is 1:1 line, and the dashed lines are 20% relative difference lines. Colors represent the relative density of the data points normalized by the maximum data density of each panel. The relative error showed in the figure is mean value \pm one standard deviation.

References

- Bond, T. C., Doherty, S. J., Fahey, D. W., Forster, P. M., Berntsen, T., DeAngelo, B. J., Flanner, M. G., Ghan, S., K^orcher, B., Koch, D., Kinne, S., Kondo, Y., Quinn, P. K., Sarofim, M. C., Schultz, M. G., Schulz, M., Venkataraman, C., Zhang, H., Zhang, S., Bellouin, N., Guttikunda, S. K., Hopke, P. K., Jacobson, M. Z., Kaiser, J. W., Klimont, Z., Lohmann, U., Schwarz, J. P., Shindell, D., Storelvmo, T., Warren, S. G., and Zender, C. S.: Bounding the role of black carbon in the climate system: A scientific assessment, *J. Geophys. Res. Atmos.*, 118, 5380-5552, 10.1002/jgrd.50171, 2013.
- Cotterell, M. I., Willoughby, R. E., Bzdek, B. R., Orr-Ewing, A. J., and Reid, J. P.: A complete parameterisation of the relative humidity and wavelength dependence of the refractive index of hygroscopic inorganic aerosol particles, *Atmos. Chem. Phys.*, 17, 9837-9851, 10.5194/acp-17-9837-2017, 2017.
- Hanel, G.: The real part of the mean complex refractive index and the mean density of samples of atmospheric aerosol particles, *Tellus*, 20, 371-379, 10.3402/tellusa.v20i3.10016, 1968.
- Kuang, Y., Zhao, C., Tao, J., Bian, Y., Ma, N., and Zhao, G.: A novel method for deriving the aerosol hygroscopicity parameter based only on measurements from a humidified nephelometer system, *Atmos. Chem. Phys.*, 17, 6651-6662, 10.5194/acp-17-6651-2017, 2017.
- Kuang, Y., Zhao, C. S., Zhao, G., Tao, J. C., Xu, W., Ma, N., and Bian, Y. X.: A novel method for calculating ambient aerosol liquid water content based on measurements of a humidified nephelometer system, *Atmos. Meas. Tech.*, 11, 2967-2982, 10.5194/amt-11-2967-2018, 2018.
- Ma, N., Zhao, C. S., Nowak, A., Müller, T., Pfeifer, S., Cheng, Y. F., Deng, Z. Z., Liu, P. F., Xu, W. Y., Ran, L., Yan, P., Göbel, T., Hallbauer, E., Mildnerberger, K., Henning, S., Yu, J., Chen, L. L., Zhou, X. J., Stratmann, F., and Wiedensohler, A.: Aerosol optical properties in the North China Plain during HaChi campaign: an in-situ optical closure study, *Atmos. Chem. Phys.*, 11, 5959-5973, 10.5194/acp-11-5959-2011, 2011.
- Ma, N., Zhao, C. S., Müller, T., Cheng, Y. F., Liu, P. F., Deng, Z. Z., Xu, W. Y., Ran, L., Nekat, B., van Pinxteren, D., Gnauk, T., Müller, K., Herrmann, H., Yan, P., Zhou, X. J., and Wiedensohler, A.: A new method to determine the mixing state of light absorbing carbonaceous using the measured aerosol optical properties and number size distributions, *Atmos. Chem. Phys.*, 12, 2381-2397, 10.5194/acp-12-2381-2012, 2012.
- Shettle, E. P., and Fenn, R. W.: Models for the Aerosols of the Lower Atmosphere and the Effects of Humidity Variations on Their Optical Properties, *Environmental Research Papers*, 676, 89, 10.1109/TR.1987.5222381, 1979.
- Wex, H., Neusüß, C., Wendisch, M., Stratmann, F., Koziar, C., Keil, A., Wiedensohler, A., and Ebert, M.: Particle scattering, backscattering, and absorption coefficients: An in situ closure and sensitivity study, *J. Geophys. Res. Atmos.*, 107, LAC 4-1-LAC 4-18, 10.1029/2000JD000234, 2002.
- Zhao, G., Zhao, C., Kuang, Y., Tao, J., Tan, W., Bian, Y., Li, J., and Li, C.: Impact of aerosol hygroscopic growth on retrieving aerosol extinction coefficient profiles from elastic-backscatter lidar signals, *Atmos. Chem. Phys.*, 17, 12133-12143, 10.5194/acp-17-12133-2017, 2017.

Zhao, G., Zhao, C., Kuang, Y., Bian, Y., Tao, J., Shen, C., and Yu, Y.: Calculating the aerosol asymmetry factor based on measurements from the humidified nephelometer system, *Atmos. Chem. Phys.*, 18, 9049-9060, 10.5194/acp-18-9049-2018, 2018.